Phase diagram of carbon at high pressures and temperatures

Matthew P. Grumbach*
Department of Physics and Materials Research Laboratory, University of Illinois at Urbana-Champaign, Urbana, Illinois 61801 and Department of Physics and Astronomy, Arizona State University, Tempe, Arizona 85287-1504

Richard M. Martin
Department of Physics and Materials Research Laboratory, University of Illinois at Urbana-Champaign, Urbana, Illinois 61801
(Received 26 February 1996)

We have made a systematic study of solid and liquid phases of carbon over a wide range of pressures and temperatures using first-principles molecular dynamics. Our simulations elucidate three aspects of the phase diagram: (1) the melting of the simple cubic phase at 35–40 Mbar; (2) structural changes in the liquid in the range of 4–10 Mbar; and (3) the melting of the BC-8 phase at ~22 Mbar. We combine the results of these three investigations to construct a proposed phase diagram for carbon. In particular, we find that above ~6 Mbar the liquid state has approximately sixfold coordination, and, consequently, that the melting temperatures of the solids in this pressure range tend to decrease with increasing pressure. [S0163-1829(96)07642-4]

I. INTRODUCTION

Carbon is unique among the elements in the diversity of its different phases.[1,2] The diamond phase is a three-dimensional tetrahedral network of fourfold coordinated atoms and is the hardest known material. The graphite phase is made up of planes of threefold coordinated atoms and is the strongest two-dimensional material known, but behaves as a lubricant because of the weak bonding between planes. The vapor consists of chains of twofold coordinated atoms.[3] The properties of other phases, such as the liquid or the proposed high-pressure metallic solid, are unknown because of the extreme conditions of temperature and pressure that are needed to study them experimentally. Although there has often been theoretical speculation about these phases, predictions have been hampered by the lack of a comprehensive model for covalent liquids.

Density-functional based molecular[4–6] dynamics provides just such a comprehensive model. The density-functional treatment of the electronic degrees of freedom allows an accurate description of all the types of bonding that might occur in carbon, while molecular dynamics offers a means to simulate various thermodynamic states. One of the most impressive applications of this method has been to help establish the nature of the melting of the diamond phase of carbon. This has led to a revision of our understanding of the phase diagram of carbon. Prior to about 1980, the proposed melting curve of the diamond phase was based on early experimental[7,8] and theoretical work,[9] and on a simple analogy with the phase diagrams of silicon and germanium, which exhibit melting curves with a negative slope in the T-P phase diagram. Recent experimental work[10–12] together with density-functional molecular dynamics[13] has clearly indicated that the slope of the line is positive. This has important consequences for theories of the Earth's interior, implying that any free carbon within the earth's interior will exist as diamond and not liquid.

The goal of this work is to investigate possible new phases of carbon at very high pressures. Many aspects of this region of the phase diagram are open to question. Does the melting point of diamond ever reach a maximum? What is the nature of the melting of the metallic phase? Does carbon really form simple cubic and BC-8 phases at high pressure, as has been proposed from previous calculations on a few structures? Does the liquid at high pressure differ substantially from the liquid examined previously at 1 Mbar? If so, could there possibly be a liquid-liquid phase transition at some intermediate pressure?

In order to answer some of these questions, we have performed a series of first-principles molecular dynamics simulations on carbon at a variety of temperatures and pressures. Our methods, described in Sec. III, include improvements over the methods used in prior work of Galli *et al.*, however, our overall strategy has been to streamline the calculations in order to investigate several different areas of the phase diagram. Since no experimental work and very little theoretical work has been previously reported for the phases that we are investigating, we need to consider a large range of conditions and investigate many cases. Therefore we have employed a minimal basis set in order to reduce the computation time needed. Since this is the most significant approximation made in this work, we have performed extensive tests in order to assure that it is physically reasonable (Appendix). In Sec. IV we study the melting of the simple cubic crystal at 35–40 Mbar. In Sec. V we investigate a pressure-induced structural change in the liquid in the range 4–10 Mbar, in Sec. VI the melting of the BC-8 crystal at ~22 Mbar. Finally in Sec. VII we combine our results to obtain a new picture of the carbon phase diagram at high pressures.

II. SURVEY OF THE CARBON PHASE DIAGRAM

The thermodynamic properties of carbon have been studied for many decades. The current picture for the phase diagram of carbon for low pressures (less than 1 Mbar) is shown in Fig. 1. The only well-known phases are the diamond and graphite solids and the vapor. Very little is known experimentally about the liquid and the boundaries drawn with

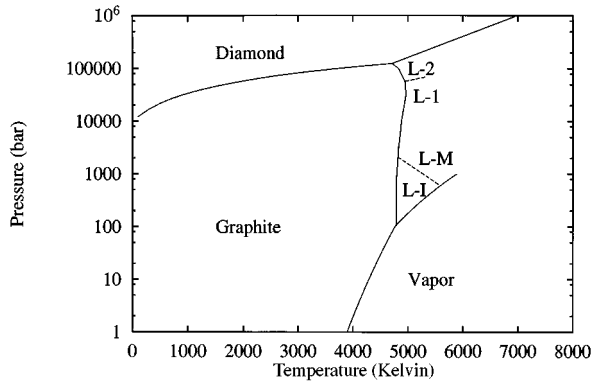

FIG. 1. Phase diagram of carbon at low pressures. Solid lines indicate phase boundaries for which some experimental evidence exists (Ref. 14). Dashed lines indicate theoretically proposed phase boundaries: liquid insulator (L-I) to liquid metal (L-M) (Ref. 15) and graphitelike liquid (L-1) to diamondlike liquid (L-2) (Ref. 16).

dashed lines in Fig. 1 are theoretical speculations, as discussed below.

Ever since it became known that diamond and graphite are polymorphs of the same material there has been great interest (both scientific and commercial) in observing the phase transition between them as pressure is applied. Beginning at the turn of this century each development of a new technique for high-pressure research was soon followed by an application to graphite. All attempts to observe the conversion to diamond under pressure at room temperature have failed, leading one investigator to conclude, ''graphite is nature's best spring.''[17] The difficulty is explained by the dramatically different bonding present in the two structures.

In the 1950s conversion was successfully obtained by using a combination of pressure, temperature, and catalysts. The use of transition-metal catalysts to lower the activation barrier will allow conversion at temperatures between 1200 and 2800 K and pressures between 50 and 90 kbar. This has given rise to an entire industry devoted to the manufacture of industrial grade diamond products. The direct conversion without catalysts was achieved[8] in the 1960s by applying temperatures greater than 3000 K to a sample under hydrostatic pressures greater than 100 kbar. Shock compression experiments have also been reported to effect the conversion.[18]

The graphite-diamond equilibrium line is the best understood part of the phase diagram.[19] For $T<1200$ K the boundary is evaluated from measured thermodynamic data of the separate phases. For 1200 K$<T<$2800 K the transition pressure can be directly observed from the catalyzed experiments, while for $T>2800$ K the uncatalyzed experiments provide the information. The phase boundary ends in a triple point at a well established pressure of 120 kbar and a less well established temperature of 4000 K.[2]

In contrast to the graphite-diamond phase line, the behavior of graphite at high temperatures has been controversial.[1,16] This stems primarily from the difficulty of performing experiments under such extreme conditions and interpreting the results. One controversy has concerned the existence of a carbyne form of solid carbon which might be thermodynamically stable at high temperatures.[20,21] The proposed carbyne form is characterized by triple bonds and two-fold coordination. This resembles the known vapor phase which consists of chains of various lengths. Since the low-pressure region is not the subject of this work, we will not discuss this conjectured phase further.

Two attempts to measure the entire melting curve have been made.[22,23] These two experiments give similar results, but differ in detail, most notably in the position assigned to the graphite-diamond-liquid triple point. Both of these involve heating by discharging a large electrical current through the carbon sample, which is contained inside a high-pressure apparatus. The resistance of the sample is monitored directly and the sudden drop observed when the applied energy goes beyond a threshold value is taken to signal a phase transition. In the first experiment[22] temperature is calculated from the amount of power delivered to the sample, while in the second experiment[23] temperature is evaluated from the ratio of observed intensities of spectral lines. Measurements were taken at pressures of 10–100 kbar.

Motivated by a theoretical prediction[15] that two phases of liquid carbon, one insulating and one metallic (see Fig. 1), may exist, more recent experiments have focused on establishing the electronic nature of the liquid at low pressures. Again, due to the difficulties in performing experiments under extreme conditions, many contradictory results have been reported. Shaner[24] has applied electrical discharge heating to glassy carbon rods up to temperatures of 6000 K at 4 kbar pressure and observed a slow *increase* of resistivity with temperature. A similar experiment with similar results has been performed by Baitin *et al.*.[25] In contrast, Heremans *et al.*.[26] have applied electrical pulses to pyrolytic graphite fibers and find a definite *drop* in resistance. They estimate that the local pressure of their sample was less than 40 bars and that the resistivity of the liquid state was in the metallic range.

Another experimental method uses a high intensity laser pulse to heat a small area of a carbon sample. A second probe beam then measures the reflectivity of the heated area. An experiment of this kind was performed by Venkatesan *et al.*[27] who reported that material ejected from the sample following the laser pulse fouled the optical equipment. In order to complete the measurement before this happens, picosecond pulses were then used. Malvezzi *et al.*[28] found a decrease in resistivity following the pulse, while Heremans *et al.*[26] found an increase. This contradiction has been recently explained by Reitze *et al.*,[29] who have used 90-fs laser pulses followed by optical measurements of 10 fs time resolution. They find that the reflectivity increases during the first 1-2 ps after the pulse but then after about 10 ps decreases to below initial reflectivity (prior to the pulse). They argue that the initial increase in reflectivity is due to a phase change to the liquid, while the decrease is due to hydrodynamic expansion of the surface. They estimate a moderate resistivity for the liquid phase from the reflectivity data, for which the title ''metal'' is barely applicable.

A difficulty of the laser-pulse approach is that it is difficult to estimate the temperature and pressure of the excited state of the sample. The experiments are done on such a short time scale that there is very little expansion of the volume of the heated material. Thus the pressure of the sample must be estimated from the temperature, which itself is also inferred. The final conclusion is that the nature of the liquid state is

still not fully established by experiment.

Recently there has been speculation by van Thiel and Ree[16] that there is a phase transition between two liquid phases (see Fig. 1). A model was developed which includes two liquid phases in addition to graphite and diamond solid phases. Liquid-1 has mostly graphitic character (threefold coordination) while liquid-2 has mostly tetrahedral character (fourfold coordination). Free energy formulas are estimated for each phase, as well as a strain energy to describe the mixing of the two liquids. Needless to say, in view of the controversial nature of experimental work on liquid carbon, there has not yet been any experimental confirmation of this intriguing proposal.

The location of the graphite-liquid-vapor triple point was disputed for a number of years, but both experiment[30] and theory[3] seem to be converging on 4700 K and 100 bars. This contradicts the experimental work cited above that finds that graphite liquifies at pressures less than 40 bars.

The nature of carbon at high pressures (greater than 100 kbar) has also been the subject of debate owing to the difficulty of attaining experimentally the extreme conditions needed to observe the phase changes and to the lack of a comprehensive theory able to describe the complex bonding behavior of carbon. The melting curve of the diamond phase was based on early experimental work,[7] quantum dielectric theory of electronegativity in covalent systems,[9] and simple analogy with the phase diagrams of silicon and germanium, which exhibit melting curves with a negative slope in the PT phase diagram. The existence of a dense metallic solid at pressures around 600 kbar was also postulated by analogy with silicon and germanium.[8]

This picture was brought into question by Yin and Cohen (1983).[31] Using the *ab initio* pseudopotential method, they compared the energetics of the diamond crystal structure to several possible closer-packed metallic structures at zero temperature. They predicted that among the structures they studied, diamond would first transform to simple cubic at a pressure of 23 Mbar. This work was extended[32–34] to consider complex tetrahedral structures. It was found that a distorted diamond structure called BC-8 was found to be stable versus diamond at pressures above 11 Mbar. This phase was also demonstrated to be semimetallic. These calculations all agreed that diamond was stable at much higher pressures than previously expected. It should be noted, however, that these studies were all done at zero temperature and only a few possible structures were examined.

The experiment of Shaner *et al.* (1984)[10] also cast doubt on the conjectured diamond melting curve. In this experiment a graphite sample was shock compressed to a series of high-temperature, high-pressure states. The sound velocity within the shocked material was monitored for possible discontinuous changes that would signal a first-order phase transition. From previous work it was known that graphite collapses to diamond when sample pressures reach the range 300–600 kbar. However, beyond this no further phase changes were detected up to 1.4 Mbar and 5600 K. This was interpreted to mean that diamond is in a solid state at this phase point. Since this temperature is higher than the triple point temperature, the slope of the phase boundary must be positive.

Further experimental evidence has been provided by Weathers and Bassett (1987),[11] who used pulsed laser heating to melt carbon particles placed inside at diamond anvil cell at pressures between 50 and 300 kbar. Following the pulse, the samples were removed from the anvil and the structure of the quenched phases was analyzed. They infer that the melt must contain a significant amount of sp^2 bonding and is therefore less dense then the coexisting solid phase. This would imply a positive slope for the melting curve.

Finally, a positive slope for the melting curve was also found by Galli, Martin, Car, and Parrinello (1990),[13] who simulated melting and freezing using first-principles molecular dynamics methods. Despite the difficulties associated with the persistence of metastable superheated or supercooled states, they were able to estimate that the melting temperature at pressures of approximately 1 Mbar is between 6500 and 8000 K. They also showed conclusively that upon melting the pressure of the system increases. Thus, from the Clausius-Clapeyron relation, they concluded that the slope of the melting curve is positive.

III. METHOD

The total energy of the system of interacting ions and valence electrons is given by the Kohn-Sham total energy:

$$E[\{\psi_i\},\{\mathbf{R}_I\}]=2\sum_{i=1}^{N}\int \psi_i^*(\mathbf{r})\left(-\frac{1}{2}\nabla^2\right)\psi_i(\mathbf{r})d\mathbf{r}+U[n], \tag{3.1}$$

$$U[n]=\int d\mathbf{r}V^{\text{ext}}(\mathbf{r})n(\mathbf{r}) +\frac{1}{2}\int\int d\mathbf{r}d\mathbf{r}'\frac{n(\mathbf{r})n(\mathbf{r}')}{|\mathbf{r}-\mathbf{r}'|}+E_{\text{xc}}[n], \tag{3.2}$$

$$n(\mathbf{r})=2\sum_{i=1}^{N}|\psi_i(\mathbf{r})|^2, \tag{3.3}$$

where ψ_i are the one-electron states, $\mathbf{R}_I$ are the positions of the ions, $n(\mathbf{r})$ is the electronic charge density, $V^{\text{ext}}(\mathbf{r})$ is the electron-ion interaction, and $E_{\text{xc}}[n]$ is the exchange-correlation energy computed within the local density approximation.[35,36]

Most of the simulations were carried out using 125 or 128 atoms in a cubic cell, although a few of the first simulations in the simple cubic pressure region used 64 atoms in an fcc cell. Only the Γ point was used to sample the Brillouin zone, which allowed the use of real-valued wave functions and therefore a decrease in computation time by a factor of 2. The interaction between the wave functions and the ionic cores was modeled using the Troullier-Martins pseudopotential[37] with the p channel being treated as local. The Kleinman-Bylander[38] form was used to treat the nonlocal s channel. We have used a cutoff of 20 Ry for the plane wave basis set.

Our molecular dynamics simulations are based on a fictitious Lagrangian:[4]

$$\mathcal{L}=\sum_{i=1}^{N}\frac{1}{2}(2\mu)\int d\mathbf{r}|\dot{\psi}_i(\mathbf{r})|^2+\sum_I\frac{1}{2}M_I\dot{\mathbf{R}}_I^2-E[\psi_i,\mathbf{R}_I]$$
$$+\sum_{ij}\Lambda_{ij}\left(\int d\mathbf{r}\psi_i^*(\mathbf{r})\psi_j(\mathbf{r})-\delta_{ij}\right). \quad (3.4)$$

The condition of orthonormality is a holonomic and stationary constraint. The resulting equations of motion are

$$\mu\ddot{\psi}_i(\mathbf{r},t)=-\frac{\delta E}{\delta\psi_i^*(\mathbf{r})}+\sum_k\Lambda_{ik}\psi_k(\mathbf{r},t)$$
$$=-f_iH\psi_i(\mathbf{r},t)+\sum_k\Lambda_{ik}\psi_k(\mathbf{r},t), \quad (3.5)$$

$$M_I\mathbf{R}_I=-\frac{\partial E}{\partial\mathbf{R}_I}. \quad (3.6)$$

The size of the time step, Δt, was 7.5 atomic units. The fictitious mass, μ, assigned to the electrons was $400m_e$. The physical mass of the ions was 12.01 atomic mass units. The constraint of orthonormality of the wave functions was maintained using standard methods for holonomic constraints.[39]

Several means were used to assign initial conditions to the various degrees of freedom. The initial values for the wave functions were obtained by minimizing the free energy[40] with the conjugate gradient method.[41] Only those orbitals needed to describe the ground state were retained for dynamics, which was performed using the total energy formalism. The wave functions were given an initial velocity of zero. The initial conditions for the ions were most often taken from a prior simulation. In some cases a perfect crystal structure was used to start the simulation, in which case the ions were assigned zero initial velocity. In other cases, the initial positions and velocities were generated by equilibrating a liquid simulation of particles interacting through a Yukawa potential.

The simulations are all constant-volume, constant-temperature dynamics. This means that the volume of the simulation cell was held fixed and that the Lagrangian dynamics was modified using the method of Nosé[42,43] to generate configurations representative of the canonical ensemble at a given temperature. Note that due to the finite size of the cell, fluctuations in temperature occur. The mass associated with the thermostat variable, s, has been chosen so that s oscillates on approximately the same time scale as the physical system. This period of oscillation is given by

$$\text{period}=\frac{2\pi}{\Delta t}\sqrt{\frac{Q}{E_{\text{kin}}}}. \quad (3.7)$$

We have chosen Q to give a period of $\sim 60\Delta t$.

We have also used a Nosé thermostat to maintain a constant temperature for the fictitious dynamics of the wave functions. This is necessary because the metallic nature of the systems studied here creates an adiabatic coupling between the electronic and ionic systems.[40,44] The target temperature assigned to the Nosé thermostat for the wave functions is given (in terms of the total kinetic energy) by:[45]

$$E_{\text{kin}}=4k_BT_{\text{target}}\frac{\mu}{M}\sum\langle\psi|(-\tfrac{1}{2}\nabla^2)|\psi\rangle. \quad (3.8)$$

The mass associated with this thermostat is then assigned a value that will result in oscillations with period $\sim 75\Delta t$.

The instantaneous pressure of the system is obtained from

$$P=-\frac{\partial E}{\partial V}+\rho k_BT, \quad (3.9)$$

where $\partial E/\partial V$ is given by an analytic expression.[46] It is well known that this analytic expression contains a systematic error when a reduced basis set is used. In the Appendix we derive a systematic correction which we have applied to all pressure estimates reported here.

IV. MELTING POINT OF THE SIMPLE CUBIC STRUCTURE

Our first goal is to establish the melting point of the simple cubic phase. As described in Sec. II, *ab initio* pseudopotential calculations at $T=0$ have indicated that the simple cubic phase will be stable at pressures greater than 27 Mbar. In order to achieve pressures of this order we have chosen to use a volume $V/V_0=0.300$, where V is the volume per atom of the simulation cell and V_0 is the volume per atom of diamond at equilibrium.

The first series of simulations used 64-atom simulation cells at temperatures between 4000 and 36 000 K. For temperatures 9000–36 000 K, the initial conditions were obtained by extracting the ionic coordinates and velocities from a simulation using a Yukawa interaction. This provides an unbiased starting point, since for fixed volume the resulting 12-fold-coordinated fluid structure populates the simulation cell in a uniform fashion. The 4000 K simulation used the end point of the 9000 K simulation as the initial conditions. We also performed a simulation at 2000 K which was initiated by quenching out of the 36 000 K liquid. At the start of each simulation the external temperatures associated with the Nosé thermostats were altered instantaneously to the new values. The systems were allowed to equilibrate for 1000 time steps, then statistical averages were collected for typically 1000 time steps more.

The liquid calculations ($T=$ 9000 K and above) equilibrated very quickly. This was easy to detect, since the coordination of the initial configuration was 12 atoms while the equilibrated liquids all showed substantially lower coordination. The average coordination and the constants of self-diffusion are reported in Fig. 2. We also show in Fig. 3 the radial distribution functions. We find that as the temperature is increased the first minimum of the radial distribution function becomes less well defined. We interpret this to mean that the system is becoming more like a perfect gas as the temperature increases.

When the temperature is lowered to 4000 K, we find that the system shows signs of nondiffusive behavior after 800 time steps, as can be seen from the plot of the average square displacement of the ions from their initial positions, Fig. 4. After 4000 time steps the atoms in the system are no longer diffusing, and so we regard the system to be solid. Thus we conclude that 4000 K is a lower bound for the melting temperature.

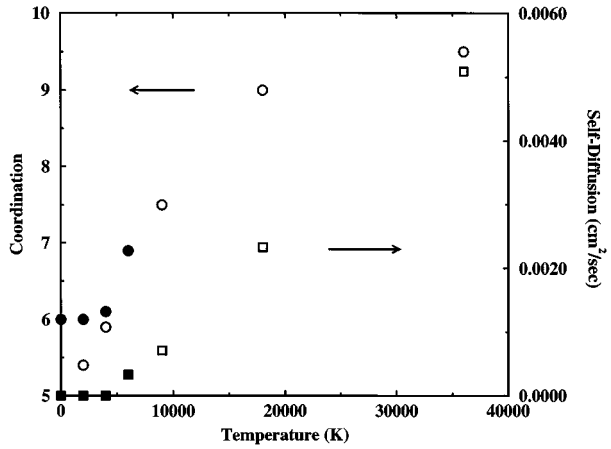

FIG. 2. Average coordination (circles) and coefficient of self-diffusion (squares) versus temperature for simple-cubic and liquid carbon at fixed volume $V/V_0=0.300$. Filled (open) symbols indicate simulations obtained by heating (cooling) a prior simulation.

More details of the solid phase were obtained from the 2000 K simulation which was initially quenched from the 36 000 K simulation. The radial distribution function and bond angle distribution function are shown in Fig. 3 and Fig. 5. We find an average coordination of 5.4 neighbors and the bond angles have a preference for 90° and 180°. This resembles a simple-cubic structure, as can be seen by comparing Fig. 3 and Fig. 5 with Fig. 6 and Fig. 7, which contain the corresponding functions for the crystalline simple cubic structure. Since we obtained a simple-cubic-like structure following a rapid quench, we conclude that simple cubic is the stable phase at these pressures. This is an important result in itself since no previous work has proven that simple cubic is even a metastable structure.

To simulate melting, another series of calculations were performed by starting from the $T=0$ perfect simple cubic crystal structure and heating up in stages to $T=$ 2000, 4000, and 6000 K. As in the above series, at each stage the external temperatures of the Nosé thermostats were readjusted instantaneously. We used a simulation cell twice as large as above, this one containing 125 atoms.

The simulation at 2000 K was observed to be solid (non-

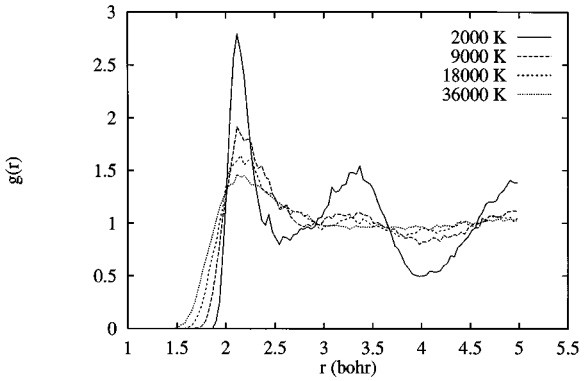

FIG. 3. Radial distribution functions for liquid carbon at high temperatures. Also shown is the radial distribution function for solid carbon at $T=2000$ K, which was obtained by quenching out of the 36 000 K liquid.

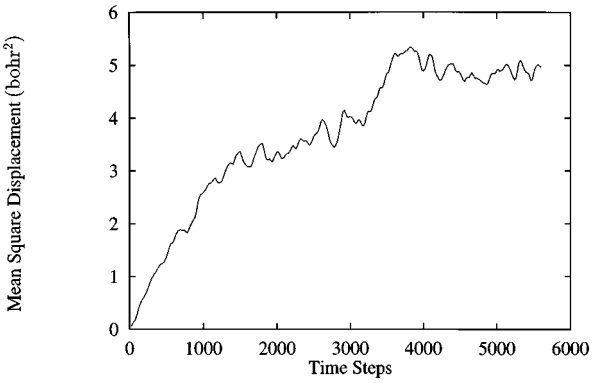

FIG. 4. Mean square displacement of the ions during simulation at 4000 K. Initially, the ions were in a liquid configuration. After 4000 time steps diffusion ceases, which is interpreted as the formation of a solid.

diffusive). The simulation at 4000 K initially began to diffuse, but after 800 time steps reverted to nondiffusive behavior, at which point we began accumulating statistical data. The 6000 K sample showed diffusion from the start, and so we can conclude this is an upper bound for the melting temperature.

The radial distribution function and the bond angle distribution function for the liquid at 6000 K are displayed in Figs. 6 and 7. We find that the liquid is similar to the solid, having coordination 6.9 and bond angles that strongly favor 90° and 180°. We believe that this sample is well equilibrated, since the measured pressure falls squarely on the equation of state for the liquid obtained in the previous series of calculations, which were all initiated from liquid configurations.

By combining the information from the two series of calculations, we can clearly establish that the melting temperature must be in the range 4000–6000 K. We found that the samples were very easy to melt or to solidify, showing very little of the hysteresis effects which often beset investigations of this kind. Furthermore, by examining the equations of state for the liquid and solid (Fig. 8) we see that in the temperature range which we have established for melting, the pressure of the liquid is always greater than that of the

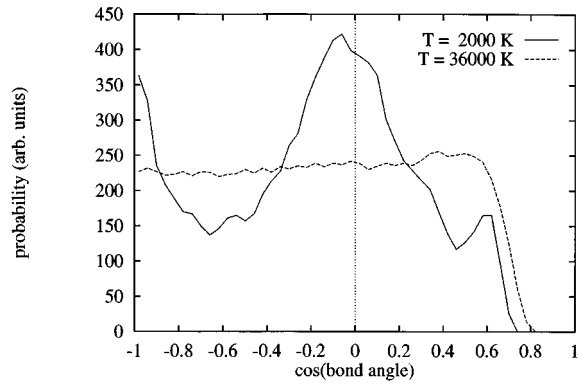

FIG. 5. Bond angle distribution function for $T=2000$ K. This sample was obtained by quenching out of the 36 000 K liquid, for which the bond angle distribution function is also shown for comparison.

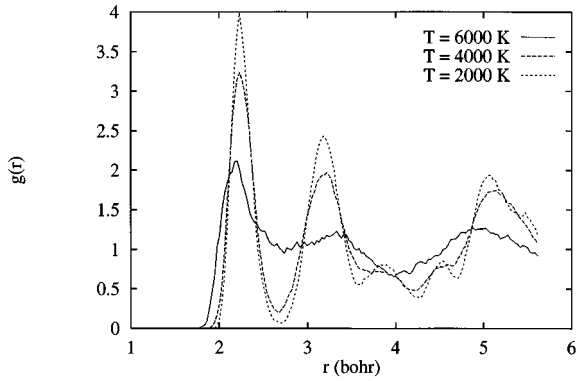

FIG. 6. Radial distribution function for simple cubic melting. Crystal at $T=2000$ K and 4000 K, liquid at 6000 K.

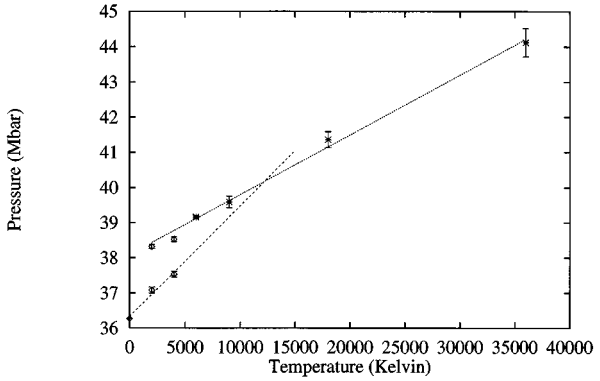

FIG. 8. Equations of state for simple cubic carbon and liquid carbon for volume fixed at $V/V_0=0.300$. * symbols represent liquid simulations. Error bars represent statistical fluctuation in the pressure.

solid at fixed volume. Using arguments based on the Clausius-Clapeyron equation

$$\frac{dP}{dT}=\frac{S_l-S_s}{V_l-V_s}, \tag{4.1}$$

we conclude that the slope of the phase line in the PT diagram must be positive. This also means that at constant pressure the liquid is less dense than the solid.

V. EVIDENCE FOR A STRUCTURAL CHANGE IN THE LIQUID

This series of simulations began with the liquid configuration obtained at the end of the 6000 K simulation discussed above. That simulation used a unit cell of volume $V/V_0=0.300$ (corresponding to a pressure of 39.2 Mbar) with 125 atoms. The final ionic coordinates and lattice constant were multiplied by a scale factor, resulting in a new volume. Simulations were performed at a series of successively larger volumes, in each case the end point of the previous simulation was scaled to obtain the initial conditions for the next. For the volume $V/V_0=0.600$, we performed an additional simulation by starting from a simulation at larger volume and decreasing the volume.

The measured coordination numbers are presented in Fig. 9. As can be seen, at low enough pressures a fourfold coordinated phase appears. However, by examining the coefficient of self-diffusion (shown in parentheses) we find that the onset of fourfold coordination at $P=$ 3.79 Mbar corresponds to a simulation which exhibited *liquid* behavior.

A fuller representation of the structural change is shown in Fig. 10, where we have plotted the radial distribution functions obtained from the six simulations. In order to compare the distribution functions obtained at different volumes, we have measured the radial coordinates in units of a length, $\sqrt[3]{V/N}$, characteristic of each volume. We find that the simulations at higher pressure exhibit a nearly identical structure, while the ones at lower pressure are clearly distinguished as a separate structure. A similar behavior is shown by the bond angle distribution function, shown in Fig. 11.

Simulations by Galli *et al.*[13] at $\sim$ 1 Mbar and simulations reported below on the melting of the BC-8 structure suggest that the fourfold coordinated solid phases have melting temperatures greater that 6000 K in the pressure range of 1–20 Mbar. This would imply that the simulations presented here are not in equilibrium, but instead are supercooled liquid states. To firmly establish that the two phases are thermodynamically stable, liquid simulations should be performed at temperatures where the liquid is known to be the equilibrium phase. This would require knowing the melting temperature of diamond in this pressure range. Lacking such knowledge,

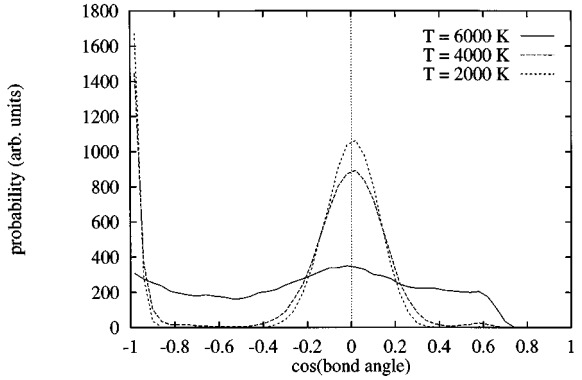

FIG. 7. Bond angle distribution function simple cubic melting. Crystal at $T=2000$ K and 4000 K, liquid at 6000 K.

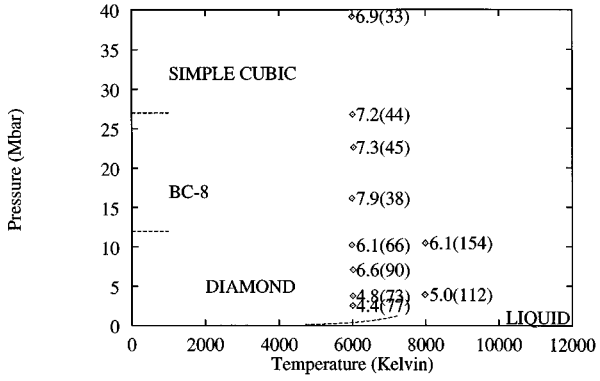

FIG. 9. Average coordination obtained from simulations. Coefficient of self-diffusion is shown in parentheses, in units of (10^{-5} cm^2/sec).

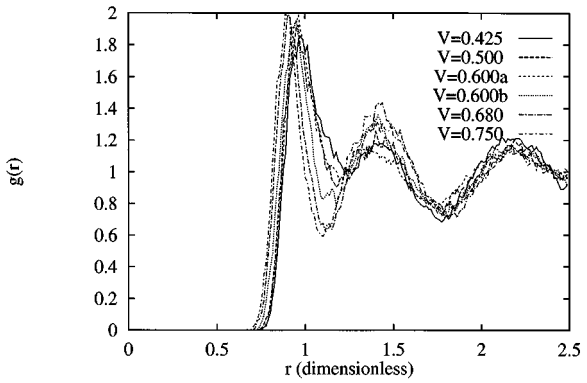

FIG. 10. Comparison of $g(r)$ for liquid carbon at various pressures. Two distinct structures are clearly exhibited. The radial coordinate for each graph has been scaled by $\sqrt[3]{V/N}$. At $V/V_0=0.600$ simulations were performed both by (a) increasing and (b) decreasing the cell volume from prior simulations.

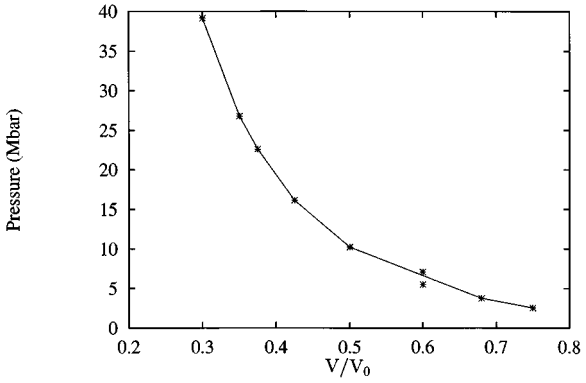

FIG. 12. Equation of state for liquid carbon $T=6000$ K. The upper point at $V/V_0=0.600$ was obtained by increasing the cell volume from a previous simulation, the lower point by decreasing the cell volume.

we have further investigated only one more temperature, 8000 K, at the two pressures which straddle the transition range, $P=$ 3.79 and 10.25 Mbar. The end points of the corresponding 6000 K simulations were used as the initial conditions. We are able to show that the structures found remain stable up to 8000 K.

Although the above results indicate the existence of two distinct phases, the existence of a first-order phase transition has not been proven. In order to demonstrate this, a discontinuity must be found in the equation of state. The phase points that have been determined by the above simulations are shown in Fig 12. In order to show a discontinuity the equations of state of the two phases must be extended into the region where the transition is expected to occur. However, we are not able to study nonequilibrium states of each of the two liquids, because of the fast time scale upon which the liquids can change their local structures.

In order to search for anomalies in the transition region near $V/V_0=0.6$, we have carried out two different simulations at this volume with different starting configurations derived respectively by scaling the coordinates of the atoms from (a) the next smaller volume where the coordination is close to sixfold, and (b) the next larger volume where the coordination is approximately fourfold. In case (a) we continue to find a simple-cubic-like structure, but with an anomalously high pressure. In case (b) we find an intermediate type of coordination, indicated by the intermediate radial distribution function in Fig. 10. This difficulty to equilibrate the atomic configurations is much more severe than at any other volume, where analogous calculations led to very similar distributions. Since this is a behavior often seen in simulations near phase transitions, these results suggest there may be a first-order phase transition near $V/V_0=0.6$; however, more definitive evidence for a true first-order phase transition must await further studies.

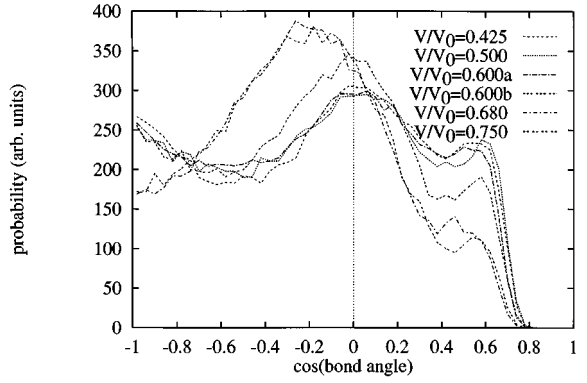

FIG. 11. Comparison of bond angle distribution function for liquid carbon at various pressures. Two distinct structures are clearly exhibited. At $V/V_0=0.600$ simulations were performed both by (a) increasing and (b) decreasing the cell volume from prior simulations.

VI. MELTING POINT OF THE BC-8 STRUCTURE

Our study of the melting of the BC-8 structure begins with the perfect crystal structure. The volume of the unit cell was chosen to be $V/V_0=0.375$. We then performed simulations at a series of progressively higher temperatures until diffusive behavior was observed.

The BC-8 structure is characterized by an internal displacement parameter, x. To fully determine the crystal structure, the total energy must be optimized with respect to this parameter. We did not perform this optimization on our initial structure, but instead estimated x by linearly extrapolating from the values reported by Fahy and Louie.[34] This gives $x=0.105$, which corresponds to bond angles of 97.4° and 118.4°. This structure was used as the initial condition for the first finite-temperature calculation at 2000 K. During this simulation we observed the bond angles to relax to values even more distorted from tetrahedral, the averages being 93.4° and 120°. Further study would reveal whether this structural relaxation is the result of the applied pressure, or the result of the finite temperature, or an artifact of the reduced basis set being used.

Simulations at $T=$ 2000, 4000, 6000, and 8000 K all remained nondiffusive (solid) throughout the simulation. The computed pressures are plotted as a function of temperature in Fig. 13. We find the usual linear equation of state which is expected for classical systems. Melting was not induced even when a vacancy and an interstitial atom were introduced into the 8000 K simulation. The system first becomes diffusive at

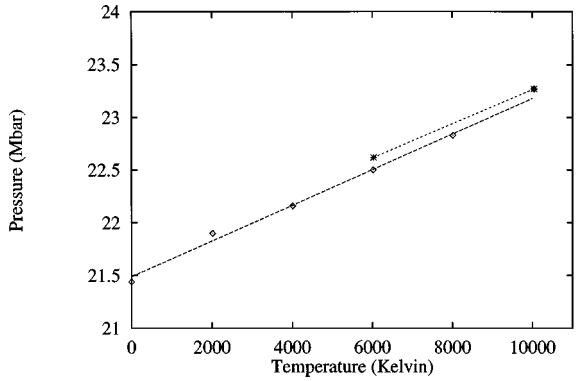

FIG. 13. Equation of state for BC-8 and its melt. Simulations marked with * are in the liquid phase.

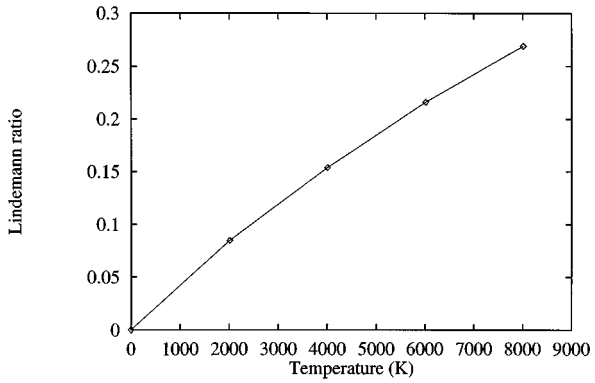

FIG. 15. Lindemann ratio versus temperature for the BC-8 structure.

10 000 K, which is therefore an upper bound to the melting temperature at this volume. Although the radial distribution function, shown in Fig. 14, does not show a well-defined second minimum, it is consistent with the fluid found at higher pressures. We estimate that the coordination is 8.6 neighbors.

We computed the pressure during the 10 000 K simulation and compared it to the equation of state for the solid (see Fig. 13). The results indicate that there is little change in pressure as the system transforms from solid to liquid. To ensure that constant pressure is not an artifact of the initial conditions of the simulation, we have simulated the liquid beginning from a completely different ionic configuration. This configuration was obtained by scaling the simulation cell and ionic velocities of the liquid simulation done at $T=6000$ K and $V/V_0=0.350$. We find that the initial conditions have no effect on the results, and in particular that the same pressure value is obtained. This shows that the liquid simulations are well equilibrated.

An estimate of the melting temperature can be found using the Lindemann melting criterion.[47] For each of the solid simulations we have computed the ratio of the root-mean-squared displacement of the atoms to the nearest-neighbor distance. The results are shown in Fig. 15. Assuming a critical Lindemann ratio of 0.15, we estimate that the melting occurs at about 4000 K.

The pressure change that we observe is small (~ 0.1 Mbar) compared to what was observed above (~ 1 Mbar) for the melting of the simple cubic structure. Because of this, we predict that the phase boundary is nearly vertical in the PT diagram. This implies that at constant pressure the liquid and the solid have similar density.

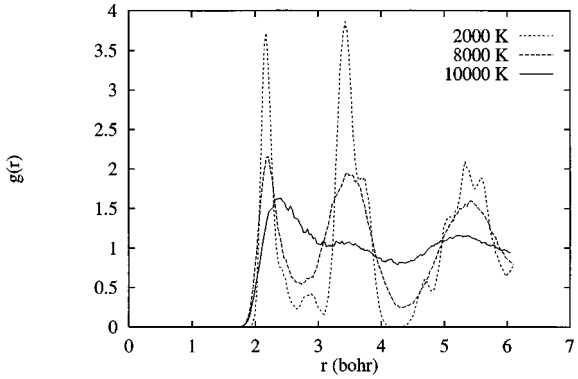

FIG. 14. Radial distribution functions for the melting of BC-8. Temperatures as indicated.

VII. DISCUSSION

We have performed an extensive series of simulations on elemental carbon using the first-principles molecular dynamics method, resulting in significant additional information on the phases at high temperatures and pressures. Previous work[32,34,33] has studied the simple cubic structure at zero temperature, but has not established that it is even metastable. Our simulations provide strong evidence that simple cubic is the thermodynamically stable structure for carbon in the range 35–40 Mbar. When the perfect crystal is heated, the structure is dynamically stable. This indicates that the structure is a local minimum of the Born-Oppenheimer surface. When the liquid is quenched to form the solid, we obtain a disordered solid with features that resemble the simple-cubic structure. Since the quenching procedure tends to find structures that are close to the global minimum, this offers some evidence that simple cubic is the *global* minimum of the Born-Oppenheimer surface and would therefore be the thermodynamically stable structure. To test this conclusion rigorously would require a long and costly simulated annealing procedure.[48]

At 20 Mbar we find that the BC-8 structure is dynamically stable, and is therefore at least metastable thermodynamically. When the perfect crystal is heated, we find that the simulation retains the BC-8 structure with bond angles of about 95° and 120°, which are consistent with internal displacement value, $x=0.125$. This value is much greater than that found by earlier work at lower pressures.[33,34] This result may be due to the effects of finite temperature or of high pressure. It is also possible that this finding may be due to the reduced basis set being used. Further investigation is needed.

We have performed molecular dynamics simulations on liquid carbon at pressures above 11 Mbar, where diamond is no longer expected to be stable. Previous theoretical work on the liquid in this pressure regime was the work of Young and Grover,[49] which was based on estimations of the free energies of the various phases and made no predictions of structure. We find that the solid and liquid phases equilibrate

quickly, showing very little hysteresis across the phase boundary. We predict that the liquid has simple-cubic character, with approximately sixfold coordination and bond angles which prefer 90° and 180°. This is in contrast to the liquid at pressures $\leqslant 1$ Mbar, which is known to have fourfold coordination,[13] but similar to silicon and germanium, which are known experimentally to have sixfold coordination.[50,51] We find this basic structure in the liquid over a wide range of pressures, 10–40 Mbar. As the liquid is heated, the average coordination increases and the bond angle distribution becomes more uniform.

Transitions between several of the phases discussed above have been investigated. We find very clear evidence that the melting temperature of the simple cubic solid at ~ 38 Mbar is between 4000 and 6000 K. We also find a definite increase in pressure upon melting at constant volume, which implies that the slope of the phase boundary in the PT phase plane is positive. Our study of the BC-8 structure yielded less definite results due to the strong hysteresis effects which made the study difficult. We were able to determine that the melting temperature at ~ 22 Mbar is between 6000 and 10 000 K and that the slope of the phase boundary, dT/dP, is very near to zero.

We have also found that the character of the liquid changes from about fourfold to about sixfold coordination in the pressure range 4–10 Mbar. This could occur either as a rapid but continuous change of a single phase or discontinuously at a first-order phase transition. Due to the difficulties of finding a discontinuity in the equation of state and to the lack of knowledge of the melting temperature of diamond at these pressures, we are unable to directly identify a first-order phase transition. Determining this would be of great interest, since phase transitions between amorphous phases are uncommon.[52–54] However, we do find two distinct liquid structures among the metastable simulations which we performed. We conclude from this that sixfold structures are unstable at pressures below ~ 6 Mbar. We further predict that this change in characteristic coordination of the liquid is associated with a change in slope of the diamond melting curve. This is based on the fact that the sixfold liquid is more dense than the fourfold liquid, and so we expect that the slope of the phase boundary between diamond and the sixfold liquid will be algebraically less than the slope of the diamond–fourfold boundary.

The features that we can add to the phase diagram are the simple-cubic-like structure of the liquid at high pressure, the position and the sign of the slope of the simple cubic crystal to liquid transition, structural change in the liquid in the pressure range 4–10 Mbar, and the position and the sign of the slope of the BC-8 to liquid transition .

Features which we infer are the following: change in the slope of the diamond-liquid phase boundary in the pressure range 4–10 Mbar, and negative slope for the diamond-liquid phase boundary near the diamond–BC-8–liquid triple point. This last feature can be inferred from our knowledge that BC-8 is denser than diamond at zero temperature and that BC-8 has about the same density as the liquid at 22 Mbar. If we can assume that these relations also hold true near the diamond–BC-8–liquid triple point, then it follows that diamond is less dense than the liquid.

We have drawn a proposed phase diagram in Fig. 16 together with several physical landmarks. The conditions we have been studying are intermediate between the conditions that occur inside the Earth and the ones that occur inside Jupiter and so are primarily of interest to the planetary sciences. We have also compared our prediction of the diamond-liquid phase boundary with that made by Young and Grover (1987).[49] In their model the free energy of the solid (derived from a lattice vibration model) is compared to the free energy of the liquid (derived from a nearly-free-electron model) to obtain the equilibrium curve. They predict that the melting temperature continues to increase with increasing pressure beyond 6 Mbar. We speculate that the discrepancy from our results at high pressures is due to the fact that their model does not include the change in the nature of the liquid that we find at 4–10 Mbar.

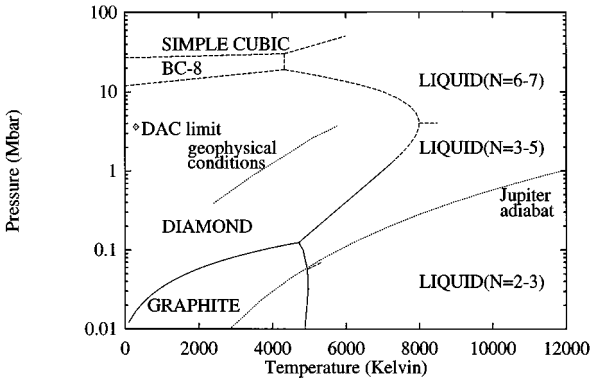

FIG. 16. Proposed phase diagram for carbon compared to other thermodynamic data. Boundaries for which some experimental data exist are shown with solid lines. Theoretical predictions are shown with dashed lines. ''DAC limit'' indicates highest pressure attained to date with a diamond anvil cell. The Jupiter adiabat continues to 35 000 K and 32 Mbar.

Some of the earlier theories of the melting of diamond were based on the belief that phase relations of carbon would be analogous to those of silicon. This led to the (erroneous) prediction that the slope of the melting curve was negative at all pressures. However, in view of our proposed phase diagram, we would like to revive the notion of an analogy between the phase diagrams of the two elements. The phase diagram of silicon exhibits the following basic features: the structure at low temperatures and pressures is tetrahedral; the tetrahedral structure transforms under pressure to a sixfold coordinated metallic structure; both solid structures melt to give a sixfold coordinated liquid; the melting temperature of the tetrahedral structure decreases with increasing pressure; the melting temperature of the metallic structure increases with increasing pressure. Based on the results of our simulations, we believe that each of these statements can also be applied to carbon at pressures above ~ 6 Mbar, if we take ''tetrahedral'' to signify both the diamond and BC-8 structures. The key to this proposal is the sixfold coordinated liquid which we find to exist over a wide range of pressures. The existence of this liquid structure at high pressures has not been previously proposed and so has not been included in previous models such as that of Young and Grover. Thus we conclude that the phase diagram of carbon, in the pressure and temperature regime relevant to planetary physics,

has significant similarities to that of silicon at lower pressures and temperatures.

ACKNOWLEDGMENTS

This research received financial support from the National Science Foundation under Grant No. DMR-89-20538, PHYS89-04035, and DMR-91-21570. Computations were performed at the Center for Computation of the Materials Research Laboratory and at the National Center for Supercomputing Applications. We thank Giulia Galli for invaluable assistance during the initial stages of this project. We thank Eric Shirley, Nithayanathan Chetty, Roberto Car, Detlef Hohl, Xiao-Ping Li, and David Drabold for helpful discussions.

APPENDIX: TESTS OF THE PSEUDOPOTENTIAL

The primary approximation that is made in this work is the use of a minimal basis set, determined by the plane wave cutoff energy of 20 Ry. Here we will demonstrate that this cutoff is sufficient to provide quantitative results.

For comparison, we have generated three pseudopotentials, two using the method of Troullier and Martins[37] (TM) and one using the method of Hamann, Schlüter, and Chiang[55] as modified by Vanderbilt[56] (HSC-V). The reference configuration used for the full atomic calculation was $1s^2 2s^2 2p^{0.5} 3d^{0.5}$. The cutoff radii used for the first TM pseudopotential were $r_{cs}=1.50$, $r_{cp}=1.54$, and $r_{cd}=1.60$ Bohr. This potential will be referred to as TM-smooth and is the one that is used in all the simulations. Another pseudopotential was generated using the same method but with $r_{cs}=0.80$, $r_{cp}=0.80$, and $r_{cd}=1.00$ Bohr. This potential will be referred to as TM-sharp. Finally we have used the HSC-V prescription with core radii $r_{cs}=0.80$, $r_{cp}=0.80$, and $r_{cd}=1.00$ Bohr to generate a third potential. The TM-smooth and HSC-V potentials are both good candidates for use in large scale calculations since they are both smooth, i.e., the potentials and wave functions are well described by a modest number of Fourier components. This will be demonstrated by the crystal calculations below. The TM-sharp potential, because of the small core radii used to define it, requires larger Fourier expansions. However, when a large enough basis set is used, we expect the TM-sharp potential to give more accurate results than TM-smooth for systems at pressures so high that the TM-smooth core radii are overlapping. Thus our purpose in examining TM-sharp is to make accurate predictions against which we can compare the predictions of TM-smooth.

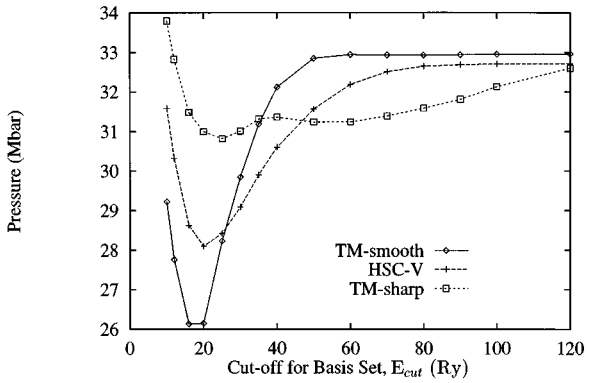

FIG. 18. Pressure as a function of $E_{\rm cut}$ of the simple cubic phase at volume $V/V_0=0.300$, as predicted by the three pseudopotentials.

The crystal calculations were performed using a program based on direct and iterative techniques for the diagonalization of the Hamiltonian. Only the *s* channel of the pseudopotential was treated as nonlocal. Both the diamond structure (2 atoms per unit cell) and the simple cubic structure (1 atom per cell) were examined at $V/V_0=0.300$. For the simple cubic structure this results in an interatomic distance of 2.3 Bohr. Brillouin zone summations were computed using ten special *k* points in the irreducible zone for diamond, and four points for simple cubic.

For a series of cutoffs, $E_{\rm cut}$, we evaluate the force on a displaced atom (Fig. 17), the value of the pressure for the perfect crystal (Fig. 18), and the energy difference between simple cubic and diamond at high pressure (Fig. 19). In these tests we see that the TM-sharp potential converges much slower than the other two, as expected. We also find that the converged values of the various energy differences using the TM-smooth potential are very close to the converged values using the TM-sharp potential. This implies that the large core radii that define TM-smooth and result in overlap of the ionic cores do not significantly affect the results.

Our choice of $E_{\rm cut}=20$ Ry for use in our simulations is

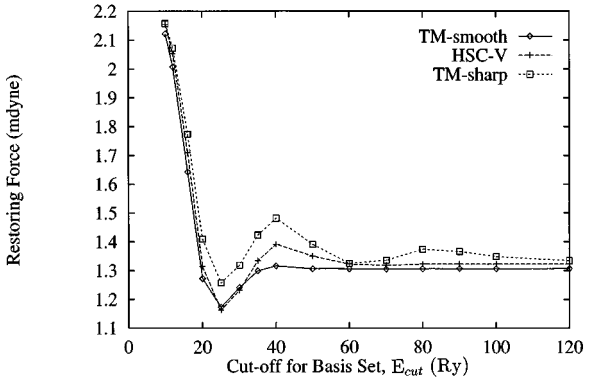

FIG. 17. Restoring force on displaced atoms as a function of $E_{\rm cut}$ for simple cubic carbon at volume $V/V_0=0.300$, as predicted by the three pseudopotentials.

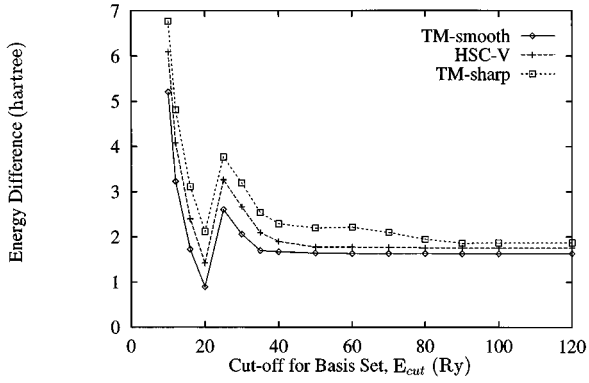

FIG. 19. Difference in energy per atom as a function of $E_{\rm cut}$ between diamond and simple cubic phases at high pressure as predicted by the three pseudopotentials.

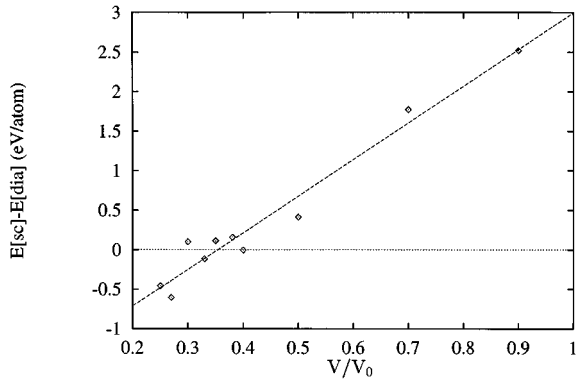

FIG. 20. Energy difference between simple cubic and diamond structures. Obtained using Troullier-Martins pseudopotential with 20 Ry cutoff for basis set. Also shown is a linear fit of the data.

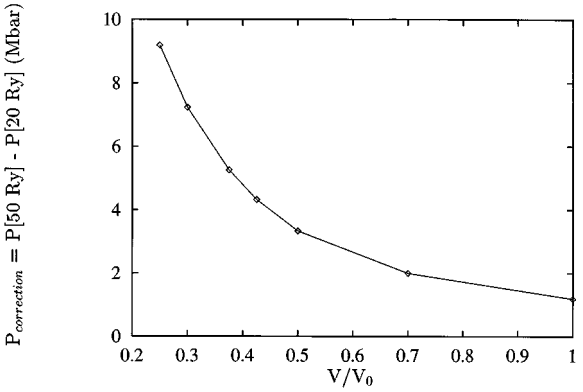

FIG. 21. Pressure correction for 20 Ry cutoff, obtained by taking the difference of 50 and 20 Ry data sets.

motivated by Fig. 17. We see that the use of this value introduces errors in the force of ~10%. As the cutoff is reduced below this the error grows rapidly. To demonstrate that this cutoff can give reasonable results, we have computed the energy difference between the simple cubic and diamond structures for a 20 Ry basis set cutoff. This time ten *k* points were used to sample the irreducible Brillouin zone for both the simple cubic and diamond structures. The results are shown in Fig. 20. The noise in the data results from using a fixed value for the cutoff, which causes the number of basis functions to change discontinuously as the volume is changed. The effects of these discontinuities can be eliminating by averaging or performing a linear fit of the data. For the hypothetical diamond to simple-cubic transformation we find a transition volume of $V/V_0 = 0.354$ under constant volume conditions. This is consistent with the results reported by Yin and Cohen,[31] who predicted a change in volume from 0.367 to 0.347 during a constant pressure transition from diamond to simple cubic. We therefore conclude that the approximation introduced by using a 20 Ry cutoff is accurate enough to predict phase transitions.

As shown in Fig. 18, a 20 Ry cutoff will introduce a significant systematic error in the calculated value of the pressure. Since an accurate measurement of the pressure is important to our work, we have devised a volume-dependent correction term to account for the error. We have calculated two equations of state for the diamond structure, one with a 50 Ry cutoff for the basis and the other with a 20 Ry cutoff. As demonstrated above, using the Troullier-Martins pseudopotential with a 50 Ry cutoff will give well-converged values for the total energy and pressure. We have tabulated the size of this error as a function of volume in Fig. 21. These values will be used as a correction to the pressures recorded during the simulations according to the following formula:

$$P = -\frac{\partial E}{\partial V} + \rho k_B T + P_{\text{correction}}. \tag{A1}$$

*Current address: Motorola Emtek Health Care Division, 1501 W. Fountainhead Pkwy., Suite 190, Tempe, AZ 85282.

[1] F. P. Bundy, Physica A **156**, 169 (1989).
[2] D. A. Young, *Phase Diagrams of the Elements* (University of California Press, Berkeley, 1991).
[3] H. R. Leider, O. H. Krikorian, and D. A. Young, Carbon **11**, 555 (1973).
[4] R. Car and M. Parrinello, Phys. Rev. Lett. **55**, 2471 (1985).
[5] D. K. Remler and P. A. Madden, Mol. Phys. **70**, 921 (1990).
[6] M. C. Payne *et al.*, Rev. Mod. Phys. **64**, 1045 (1992).
[7] B. J. Alder and R. H. Christian, Phys. Rev. Lett. **7**, 367 (1961).
[8] F. P. Bundy, J Chem. Phys. **38**, 631 (1963).
[9] J. A. Van Vechten, Phys. Rev. B **7**, 1479 (1973).
[10] J. W. Shaner, J. M. Brown, C. A. Swenson, and R. G. McQueen, J. Phys. (Paris) Colloq. **45**, C8-235 (1984).
[11] M. S. Weathers and W. A. Bassett, Phys. Chem. Miner. **15**, 105 (1987).
[12] M. Togaya, High Pres. Res. **4**, 342 (1990).
[13] G. Galli, R. M. Martin, R. Car, and M. Parrinello, Science **250**, 1547 (1990).
[14] P. Gustafson, Carbon **24**, 169 (1986).
[15] A. Ferraz and N. H. March, Phys. Chem Liq. **8**, 289 (1979).
[16] M. van Thiel and F. H. Ree, Phys. Rev. B **48**, 3591 (1993).
[17] F. P. Bundy, J. Chem. Phys. **38**, 631 (1963), attributed to P. W. Bridgeman.
[18] M. N. Pavlovskii, Sov. Phys. Solid State **13**, 741 (1971).
[19] C. S. Kennedy and G. C. Kennedy, J. Geophys. Res. **81**, 2467 (1976).
[20] A. G. Whittaker, Science **229**, 485 (1985).
[21] P. P. K. Smith and P. R. Buseck, Science **229**, 486 (1985).
[22] F. P. Bundy, J Chem. Phys. **38**, 618 (1963).
[23] N. S. Fateeva and L. F. Vereshchagin, Pis'ma Zh. Éksp. Teor. Fiz. **13**, 110 (1971).
[24] J. W. Shaner, Bull. Am. Phys. Soc. **32**, 607 (1987).
[25] A. V. Baitin *et al.*, High Temp.—High Press. **21**, 157 (1990).
[26] J. Heremans *et al.*, Phys. Rev. Lett. **60**, 452 (1988).
[27] T. Venkatesan *et al.*, Phys. Rev. Lett. **53**, 360 (1984).
[28] A. M. Malvezzi, N. Bloembergen, and C. Y. Huang, Phys. Rev. Lett. **57**, 146 (1986).
[29] D. H. Reitze, H. Ahn, and M. C. Downer, Phys. Rev. B **45**, 2677 (1992).
[30] M. A. Scheindlin, V. N. Senchenko, and A. V. Baitin, Dokl. Akad. Nauk SSSR **298**, 1383 (1988).
[31] M. T. Yin and M. L. Cohen, Phys. Rev. Lett. **50**, 2006 (1983).
[32] M. T. Yin, Phys. Rev. B **30**, 1773 (1984).
[33] R. Biswas, R. M. Martin, R. J. Needs, and O. H. Nielsen, Phys. Rev. B **35**, 9559 (1987).

[34] S. Fahy and S. G. Louie, Phys. Rev. B **36**, 3373 (1987).
[35] D. M. Ceperley and B. J. Alder, Phys. Rev. Lett. **45**, 566 (1980).
[36] J. P. Perdew and A. Zunger, Phys Rev. B **23**, 5048 (1981).
[37] N. Troullier and J. L. Martins, Phys. Rev. B **43**, 1993 (1991).
[38] L. Kleinman and D. M. Bylander, Phys. Rev. Lett. **48**, 1425 (1982).
[39] J. P. Ryckaert, G. Ciccotti, and H. J. C. Berendsen, J. Comput. Phys. **23**, 327 (1977).
[40] M. P. Grumbach, D. Hohl, R. M. Martin, and R. Car, J. Phys., Condens. Matter **6**, 1999 (1994).
[41] I. Štich, R. Car, M. Parrinello, and S. Baroni, Phys. Rev. B **39**, 4997 (1989).
[42] S. Nosé, Mol. Phys. **52**, 255 (1984).
[43] S. Nosé, J. Chem. Phys. **81**, 511 (1984).
[44] G. Pastore, E. Smargiassi, and F. Buda, Phys. Rev. A **44**, 6334 (1991).
[45] P. E. Blöchl, Phys. Rev. B **41**, 5414 (1990).
[46] O. H. Nielsen and R. M. Martin, Phys. Rev. B **32**, 3792 (1985).
[47] D. Tabor, *Gases, Liquids and Solids*, 2nd ed. (Cambridge University Press, Cambridge, 1979).
[48] W. M. Press, B. P. Flannery, S. A. Teukolsky, and W. T. Vetterling, *Numerical Recipes* (Cambridge University Press, Cambridge, 1986).
[49] D. A. Young and R. Grover, in *Shock Waves in Condensed Matter 1987*, edited by S. C. Schmidt and N. C. Holmes (North-Holland, Amsterdam, 1988), pp. 131–134.
[50] Y. Waseda and K. Suzuki, Z. Phys. B **20**, 339 (1975).
[51] J. P. Gabathuler and S. Steeb, Z. Naturforsch. Teil A **34**, 1314 (1979).
[52] S. Aasland and P. F. McMillan, Nature **369**, 633 (1994).
[53] P. H. Poole *et al.*, Phys. Rev. Lett. **73**, 1632 (1994).
[54] P. H. Poole *et al.*, Comput. Mater. Sci. **4**, 373 (1995).
[55] D. R. Hamann, M. Schlüter, and C. Chiang, Phys. Rev. Lett. **43**, 1494 (1979).
[56] D. Vanderbilt, Phys. Rev. B **32**, 8412 (1985).